L-arabinose induces the formation of viable non-proliferating spheroplasts in Vibrio cholerae

Elena Espinosa, Sandra Daniel, Sara Hernandez, Anthony Goudin, Felipe Cava, François-Xavier Barre, Elisa Galli

L-arabinose induces the formation of viable non-proliferating spheroplasts in *Vibrio cholerae*

Elena Espinosa[1#], Sandra Daniel[1#], Sara B. Hernández[2], Anthony Goudin[1], Felipe Cava[2], François-Xavier Barre[1@], Elisa Galli[1@]

[1] Institute for Integrative Biology of the Cell (I2BC), Université Paris-Saclay, CEA, CNRS, Gif-sur-Yvette, France

[2] The laboratory for Molecular Infection Medicine Sweden (MIMS), Department of Molecular Biology, Umeå University, Umeå, Sweden

[#] Elena Espinosa and Sandra Daniel contributed equally to this work. Author order was determined in order of decreasing seniority.

[@] Address correspondence to: francois-xavier.barre@i2bc.paris-scalay.fr, elisa.galli@i2bc.paris-saclay.fr

Keywords

Vibrio cholerae, spheroplasts, growth arrest, L-arabinose

Abstract

Vibrio cholerae, the agent of the deadly human disease cholera, propagates as a curved rod-shaped bacterium in warm waters. It is sensitive to cold, but persists in cold waters under the form of viable but non-dividing coccoidal shaped cells. Additionally, *V. cholerae* is able to form non-proliferating spherical cells in response to cell wall damage. It was recently reported that L-arabinose, a component of the hemicellulose and pectin of terrestrial plants, stops the growth of *V. cholerae*. Here, we show that L-arabinose induces the formation of spheroplasts that lose the ability to divide and stop growing in volume over time. However, they remain viable and upon removal of L-arabinose they start expanding in volume, form branched structures and give rise to cells with a normal morphology after a few divisions. We further show that WigKR, a histidine kinase/response regulator pair implicated in the induction of a high expression of cell wall synthetic genes, prevents the lysis of the spheroplasts during growth restart. Finally, we show that the physiological perturbations result from the import and catabolic processing of L-arabinose by the *V. cholerae* homolog of the *E. coli* galactose transport and catabolic system. Taken together, our results suggest that the formation of non-growing spherical cells is a common response of *Vibrios* exposed to detrimental conditions. They also permit to define conditions preventing any physiological perturbation of *V. cholerae* when using L-arabinose to induce gene expression from the tightly regulated promoter of the *Escherichia coli araBAD* operon.

Importance

Vibrios among other bacteria form transient cell wall deficient forms as a response to different stresses and revert to proliferating rods when permissive conditions have been restored. Such cellular forms have been associated to antimicrobial tolerance, chronic infections and environmental dispersion.

The effect of L-Ara on *V. cholerae* could provide an easily tractable model to study the ability of *Vibrios* to form viable reversible spheroplasts. Indeed, the quick transition to spheroplasts and reversion to proliferating rods by addition or removal of L-Ara is ideal to understand the genetic program governing this physiological state and the spatial rearrangements of the cellular machineries during cell shape transitions.

Introduction

Cholera is an acute diarrhoeal disease caused by ingestion of food or water contaminated with *Vibrio cholerae*, a curved rod shape bacterium that propagates in warm briny and salty waters. Cold stops *V. cholerae* proliferation. However, the bacterium has the ability to persist for months in cold water under the form of coccoid bodies and return to growth when the sea temperature rises (1–3). Similarly, *V. cholerae* is known to persist under a spherical form in biofilms (4) and to survive exposure to antibiotics inhibiting cell wall synthesis under the form of spheroplasts, i.e. a spherical cell in which the cell wall has been partially or completely removed (5).

The high propagation rate of *V. cholerae* and its capacity to survive unfavorable growth conditions have led to several pandemics, which have caused and are still causing major socio-economic perturbations (6). Seven cholera pandemics have been recorded since the beginning of the 18th century. Isolates of the current on-going pandemic, which started over 50 years ago, are rapidly drifting (7–11). It is suspected that the constant appearance of new atypical pathogenic variants of *V. cholerae* will eventually lead to a more virulent strain that will start a new pandemic, which motivated extensive research on the physiology of the bacterium and its evolution towards pathogenicity (7–11). The use of a tightly-regulated high-level expression inducible system based on the regulation of the promoter of the *Escherichia coli araBAD* operon by the AraC regulator, known as the P_{BAD} system (12), played an instrumental role in many *V. cholerae* studies (13). The AraBAD enzymes allow *E. coli* to

exploit L-arabinose (L-Ara), a component of the hemicellulose and pectin of terrestrial plants, as a carbon and energy source (14). AraC acts both as a positive and a negative regulator, repressing P_{BAD} in the absence of L-Ara and activating its transcription when bound to it (14). *V. cholerae* lacks a *bona fide* arabinose import and metabolization pathway. Nevertheless, the *E. coli* P_{BAD} system proved to be very effective in *V. cholerae*, which suggested that L-Ara was imported in the cytoplasm of the cells. However, we and others recently reported that L-Ara could interfere with the growth of *V. cholerae* (15, 16), calling for a better understanding of the impact of L-Ara on the physiology of this bacterium.

Here, we show that *V. cholerae* cells stop dividing or elongating and lose their characteristic curved rod cell shape in the presence of >1% (w/v) and >0.1% (w/v) of L-Ara in rich and poor media, respectively. *V. cholerae* cells become spherical and morphologically similar to spheroplasts obtained by exposure to cell wall targeting antibiotics (5) or to coccoid bodies formed in cold temperatures (1, 2, 17). We further found that mutants with impaired physiology are more sensitive to the presence of L-Ara, morphologically transitioning to spheroplasts with as little as 0.01% (w/v) of L-Ara in poor media. We show that the spheroplasts induced by L-Ara are able to revert to exponentially growing rods in only a few generations when L-Ara is removed, demonstrating that they remain viable. Finally, we demonstrate that L-Ara is imported and processed by the *V. cholerae* homologs of the *E. coli* galactose transport and catabolic enzymes and that one of its by-product perturbs the physiology of the cell by entering the glycolysis pathway. Taken together, these results suggest that formation of spherical cells might be a general physiological response of *Vibrios* when faced with detrimental conditions. From a technical point of view, they permit to define conditions that allow the use of the P_{BAD} expression system in *V. cholerae* while preventing any perturbation of the physiological state of the cells.

Results

L-arabinose induces the formation of non-dividing spherical cells

To study the effect of L-Ara on cell morphology and growth, we added increasing concentrations of L-Ara to wild-type N16961 *V. cholerae* in the early exponential phase in different liquid media. Cells grown in M9-MM appeared with a wild-type rod shape in the absence or up to 0.02% (w/v) L-Ara, but >90% of the cells became spherical in few hours in the presence of 0.1% (w/v) L-Ara (Figure 1A). In cultures grown in M9-MM supplemented with casamino acids (CAA), spherical cells started to appear at 0.2% (w/v) of L-Ara, and the majority of the cells became spherical at 0.5% (w/v) of L-Ara. In LB, the concentration of L-Ara had to be increased up to 1% (w/v) to induce morphological changes (Figure 1A). The spherical shape of L-Ara treated cells resembles that of non-proliferative cells obtained by treating *V. cholerae* cells with cell wall targeting antibiotics (5) or by incubating them at 4°C (2, 4), even though at cold temperatures cells appear to be smaller in size (Figure 1B).

In parallel to microscopic inspection, we followed the optical density of cell cultures over time. In all tested media, L-Ara had a detrimental effect on cell proliferation at the same concentrations at which it induced the formation of spherical cells (Supplementary Figure 1). Cell growth was inhibited shortly after the addition of L-Ara, at an optical density at which cells would have otherwise kept growing exponentially, indicating that L-Ara induced a rapid metabolic arrest (Supplementary Figure 1).

V. cholerae is known to be sensitive to high concentrations of several carbon sources, including glucose (18). None of 8 other commonly used carbon sources had similar effects on cell shape and growth, including D-arabinose (Table 1 and Supplementary Figure 2).

The L-Ara phenotype was not restricted to N16961, strain isolated in Bangladesh in the 1970s, but it was shared among the most prominent pandemic *V. cholerae* serotype O1 El Tor strains such as C6706, isolated in a cholera outbreak in Peru in the 1990s, and E7946, isolated

125 in Bahrain in 1978. A *V. cholerae* non-O1 non-139 was similarly affected by L-Ara exposure
126 (Supplementary Figure 3).

127 **Mutants with impaired physiology are more sensitive to L-Ara**

128 We had previously noticed that it was impossible to use the P_{BAD} system to produce proteins
129 of interest in a few *V. cholerae* mutants because the presence of L-Ara inhibited their growth.
130 The above results prompted us to revisit the phenotype of two of those mutants whose growth
131 was completely arrested by the addition of as little as 0.01% (w/v) of L-Ara in M9-MM: a
132 N16961 strain carrying two copies of the *ssb* gene, which codes for an essential single strand
133 DNA binding protein implicated in the regulation of replication, transcription and
134 homologous recombination repair (19), and a derivative of the MCH1 monochromosomal
135 strain, in which the SlmA nucleoid occlusion protein was overproduced (20). In both cases,
136 we observed that 0.01% (w/v) of L-Ara was sufficient to induce the formation of spherical
137 cells in the entire cell population (Figure 1C).

138 **Transition dynamics to spherical cells at the population level**

139 To visually inspect the morphological transition at the population level over time, we
140 collected cell samples every hour for 10 hours after L-Ara addition and examined them at the
141 microscope. Cells were divided in three categories based on their shape: cells with a rod
142 shape, cells composed of a rod and a small or large irregular bulge protruding from the cell
143 wall, which we refer to as bleb, and cells with a spherical shape (Figure 2A). In cell cultures
144 grown at 30°C, spherical cells started to appear after 5 hours and comprised 90% of the cell
145 population after 9 hours. The sharp increase in the proportion of spherical cells in the
146 population corresponded to an equally fast decline in rod shaped cells, which dropped to less
147 than 10% of the cell population at the end of the experiment. Blebbing cells appeared around
148 4 hours after L-Ara addition. Blebs were randomly located on the surface of the cells. In
149 particular, there was no preference for mid-cell or cell pole locations (Supplementary Figure

4). Cells with protruding blebs never represented more than 5% of the entire cell population and almost disappeared at the end of the time course, which suggested that they corresponded to a transient state between the rod and the spherical state. We refer to them as transitioning cells. Taken together, these results suggest that a few hours are required after growth arrest before morphological transition. However, once transition is initiated the formation of spherical cells is very fast.

In a similar time course experiment performed at 37°C, cells appeared to respond faster to L-Ara: the first blebs appeared 3 hours after L-Ara addition and after 5 hours about 40% of the cell population had completed transition to spherical bodies (Supplementary Figure 5).

The size of the spherical cells was heterogeneous and the diameter of the majority of cells was comprised between 1.5 and 1.8 µm (Figure 2B). The average diameter of the spherical cells did not change between the 7, 8, 9 and 10 hour time points after L-Ara addition, suggesting that once formed, spherical cells neither decreased nor increased in volume (Figure 2C). Based on the measured dimensions of spherical and rod-shaped cells, we estimate that the cell volume of spherical cells is around 2.5 times bigger than that of exponentially growing rod cells.

Transition dynamics to spherical cells at the single cell level

We performed time-lapse video-microscopy experiments to inspect the transition process from rod to sphere at the single cell level (Figure 2D and Movie 1). All the observed cells displayed the same transition pattern. After exposure to L-Ara, a single bleb appeared at the bacterial cell surface. As the bleb increased in size, the original cell was assimilated into the forming sphere until the original rod shape was completely lost. The time when a bleb became visible on the cell surface and its location varied from cell to cell. However, once started, completion of the morphological change was comparable in all cells, with the exception of a

few rare cells that lysed during the process (Movie 2). On an agarose M9-MM pad, blebbing cells transitioned to spheres in around 2 to 3 hours at 30°C (Figure 2D and Movie 1).

L-Ara induced spherical cells are cell wall deficient

The spherical shape of L-Ara treated cells is similar to cell wall deficient forms that have completely or almost entirely lost the peptidoglycan (PG) layer, which suggested a process of cell wall degradation or PG remodelling mechanism (21). To verify this point, we compared the PG content and composition of *V. cholerae* exponentially growing cells and L-Ara induced non-dividing spherical cells (Table 2). To limit contamination by the PG of cells that had not completely transformed into spheres in the presence of L-Ara, we used MCH1 cells expressing an additional copy of SlmA because they fully transitioned to spherical cells in the presence of as little as 0.01% (w/v) of L-Ara (Figure 1C).

The PG of exponentially growing cells and cells that had completely transitioned to spheres after the addition of 0.1% (w/v) of L-Ara was extracted and submitted to UPLC analysis (Supplementary Figure 6A). The area of the UPLC profiles showed that the amount of PG per cell in L-Ara treated bacteria was around 10 times lower than the amount present in rod-shaped cells (Supplementary Figure 6B). In addition, we found that glycan chains were twice shorter in L-Ara treated cells than in untreated cells. The length of glycan chains is calculated based on the number of anhydro-muropeptides (22), which results from the activity of lytic transglycosylases (23, 24). Therefore, the observed reduction in the average glycan chain length suggests an increase of lytic transglycosylase activity in the presence of L-Ara. Finally, we observed that the amount of DAP-DAP cross-linked muropeptides significantly increased in L-Ara treated cells. Taken together, these results indicate that cell wall metabolism is perturbed after L-Ara exposure and that spherical cells are almost completely deprived of the PG layer, which corresponds to the definition of a spheroplast.

L-Ara induced spheroplasts are viable

To evaluate if L-Ara had a detrimental effect on cell viability we estimated the number of viable bacteria in a time course experiment. A culture of N16961 cells was split in two after 2 hours of growth and L-Ara was added to one of the two halves. The number of viable cells in each culture was determined by plating aliquots on LB plates and counting the number of colonies. Viable cell count kinetics (represented as colony forming units, CFU) showed that L-Ara addition had an immediate inhibitory effect on cell proliferation but did not cause a corresponding decline in cell viability (Figure 3A). Indeed, 75% of the number of cells before L-Ara addition gave rise to colonies after a 10 hours incubation with L-Ara (Figure 3B).

Time-lapse video-microscopy was performed to determine how non-proliferating spherical cells could return to proliferation and recover a curved rod shape after L-Ara removal. Single cell analyses showed that reversion to proliferating rods started with the elongation of the spheroplasts, which was followed by the formation of multiple protrusions on their surface (Figure 3C and Movie 3). The protrusions elongated outward, giving rise to branched cells. Curved rod shape cells were recovered after a few division events. The time required to initiate elongation greatly differed from cell to cell: the recovery process started almost immediately after the removal of L-Ara in some cells but took a few hours to initiate in others. However, the time between the initiation of the recovery process and its completion was similar for all the cells. On an agarose M9-MM pad at 30°C, cells transitioned from elongating spheres to symmetrically dividing rods in around 4 to 5 hours. It was not necessary to add osmo-protectants in liquid or on agarose pads to avoid the lysis of spherical cells before and after the initiation of the proliferation recovery process.

Time-lapse video-microscopy observations further suggested that the overall 25% loss of CFU after 10 hours of L-Ara treatment (Figure 3B) was accounted for by the number of cells

222 that lysed during the transition to spheroplasts after the addition of L-Ara (Movie 2) and by
223 those that lysed during the recovery process after L-Ara removal (Movie 4).

224 **_wigKR_ is essential for the recovery of cells after L-Ara treatment**

225 The histidine kinase/response regulator pair WigKR (also known as VxrAB) is thought to
226 induce a higher expression of the full set of cell wall synthetic genes in response to cell wall
227 damage (25). It was previously reported that it was essential for the recovery of cell shape and
228 the return to proliferation of *V. cholerae* cells treated with cell wall targeting antibiotics (25),
229 which prompted us to inspect the effect of L-Ara on Δ*wigKR* cells. We observed no
230 differences in the growth arrest and formation of spherical cells of the Δ*wigKR* strain in the
231 presence of L-Ara (Supplementary Figure 7A). As observed before, spherical cell formation
232 initiated from a single bleb randomly distributed on the surface of the cell. However, Δ*wigKR*
233 spherical cells immediately started to grow in diameter when L-Ara was removed, expanding
234 continuously in size until they exploded (Figure 3D and Movie 5). On the contrary, Δ*wigKR*
235 cells that had not yet transitioned to spheroplasts were able to return to a proliferative state
236 without any obvious defect (Movie 6). After a 10 hours incubation with L-Ara, only 10% of
237 the Δ*wigKR* cells could still form colonies, which corresponded to the proportion of cells that
238 had not started transitioning to spheres (Supplementary Figure 7B). Taken together, these
239 results suggest that the histidine kinase/response regulator pair WigKR plays an essential role
240 in the recovery of the L-Ara induced spheroplasts.

241 **Identification of genes required for L-Ara sensitivity**

242 In contrast to cell wall targeting antibiotics, growth arrest and spheroplast formation were
243 unlikely to result from the action of L-Ara on the cell surface or in the periplasm of *V.*
244 *cholerae*. *V. cholerae* lacks a *bona fide* arabinose import and metabolization pathway, but the
245 effectiveness of the *E. coli* P_{BAD} promoter regulation by L-Ara suggested that it was at least

246 passively imported in the cytoplasm of this bacterium. To identify putative factors involved in
247 the response of *V. cholerae* cells to L-Ara, we performed two complementary genetic screens.
248 First, we employed a screen based on the enrichment of L-Ara-insensitive mutants in a cell
249 population grown in liquid in M9-MM supplemented with 0.2% (w/v) L-Ara. We constructed
250 a library of N16961 mutants with a Mariner transposon (Tn), which randomly inserts at 5'-
251 TA-3' sites (26). We grew the library in M9-MM supplemented with 0.2% (w/v) L-Ara for 18
252 hours. Aliquots were collected before L-Ara addition and after 9 and 18 hours of incubation
253 with L-Ara. Deep sequencing was used to determine all the positions at which the Tn was
254 inserted in the collected libraries. We thus identified nine genetic loci in which Tn insertions
255 were significantly overrepresented after growth in presence of L-Ara (Figure 4A). The
256 transposition frequency and insertion profile differed in the overrepresented genes (Figure
257 4B). Tn insertions covered both DNA strands of the entire gene length of *vc1325*, *vc1327*,
258 *vc1328*, *vc1595*, *vc1596* and *vc0263*, suggesting that the product of these genes was
259 implicated in the physiological effect of L-Ara. Tn insertions covered the entire length of a
260 specific DNA strand of *vc0262*, suggesting that they had a polar effect on the expression of
261 *vc0263*. The overrepresentation of Tn insertions was restricted to only one of the multiple 5'-
262 TA-3' sites present in the entire gene length of *vc0779* and *vc2621*, suggesting that L-Ara
263 insensitive phenotype could be provided by an additional suppressor mutation located at
264 another genetic locus. The suppressor capacity of the inactivation of *vc1325*, *vc1327*, *vc1328*,
265 *vc1595*, *vc1596* and *vc0263* was confirmed by using the corresponding mutants in an ordered
266 mapped Tn library of the wild-type C6706 strain (27). Inactivation of *vc1325*, *vc1327*,
267 *vc1328*, *vc1595*, *vc1596* and *vc0263* fully restored growth of C6706 in presence of L-Ara
268 (Supplementary Figure 8).
269 In addition, as L-Ara insensitive mutants presenting a growth defect cannot be identified with
270 a screen based on growth enrichment, we decided to directly plate a random Tn insertion

library on M9-MM plates containing L-Ara. To limit the number of false positives, i.e. the formation of colonies by cells still sensitive to L-Ara, we used the MCH1 strain carrying an additional copy of the *slmA* gene, which fully transitions to spheres in the presence of as little as 0.01% (w/v) of L-Ara (Figure 1C). Plating of the Tn insertion library on M9-MM plates containing 0.1% (w/v) L-Ara resulted in the formation of 11 colonies, 9 of which were confirmed to be L-Ara insensitive after re-isolation on fresh L-Ara plates. Sequencing showed that they corresponded to Tn insertions in six different genes (Table 3 and Supplementary Figure 9), five of which had already been detected in the growth enrichment screen (*vc1325*, *vc1327*, *vc1328*, *vc1596* and *vc0263*). In addition, three independent Tn hits were obtained in *vc2689*. The strain corresponding to the inactivation of *vc2689* was missing in the ordered mapped Tn library of the wild-type *V. cholerae* C6706 strain (27). Therefore, we directly engineered the mutation in the N16961 wild-type background to confirm that its inactivation suppressed the effect of L-Ara (Supplementary Figure 8). L-Ara reduced the growth rate of *vc2689* mutants (Supplementary Figure 8). However, microscopic inspection revealed a majority of rod-shaped cells and a few isolated spherical cells, suggesting that L-Ara sensitivity was reduced even though not completely suppressed.

Discussion

It was recently reported that L-Ara inhibited the proliferation of *V. cholerae* (15, 16). Here, we show that it is associated with a change in the morphology of the cells from a curved rod shape to a spherical form (Figure 1). The spherical cells lose the ability to divide and stop growing in volume over time, suggesting a major metabolic arrest (Figure 2). We found that L-Ara induced spherical cells are spheroplasts, i.e. they have almost completely lost their cell wall (Table 2 and Supplementary Figure 6). Nevertheless, they remain viable and once L-Ara is removed from the environment they resume proliferation and revert to the original cell shape after a few divisions (Figure 3).

Metabolism arrest is linked to the processing of L-Ara by the galactose pathway

We found that the addition of L-Ara almost immediately stopped *V. cholerae* proliferation in both fast and slow growing conditions, in contrast to the addition of 8 other commonly used carbon sources (Figure 1 and Table 1). *V. cholerae* lacks a *bona fide* L-Ara import and degradation pathway. However, the effectiveness of the regulation of the *E. coli* P_{BAD} promoter in *V. cholerae* suggested that it was at least passively imported in the cytoplasm of the bacterium, where it interfered with the metabolism. We performed 2 genetic screens to determine which cellular processes might be involved in the action of L-Ara.

We identified 7 genes whose inactivation suppressed the sensitivity to L-Ara (Figure 4 and Table 3). 6 of those genes can be directly (*vc1325*, *vc1327*, *vc1328*, *vc1596* and *vc1596*) or indirectly (*vc0263*) linked to the galactose Leloir catabolic pathway. *vc1325*, *vc1327* and *vc1328* code for homologues of the 3 components of the *E. coli* ABC galactose transport system, the periplasmic binding protein MglB, the ATP-binding protein MglA and the integral membrane permease MglC, respectively (28, 29). *vc1595* codes for a homologue of the *E. coli* galactokinase GalK, the first enzyme in the Leloir pathway of galactose metabolism (30). *vc1596* codes for a homologue of *E. coli* GalT, the galactose 1-phosphate uridylyltransferase. *vc0263* codes for a putative homologue of the enzyme initiating colanic acid synthesis in *E. coli*, WcaJ (31), which was also described to act as a galactose-1-phosphate transferase *in vitro* (32). These results suggest that L-Ara is imported in the cytoplasm of *V. cholerae* by the galactose transporter and processed by the galactose catabolic enzymes (Figure 5). In *Sinorhizobium meliloti*, the arabinose transporter AraABC has been described to play a role in galactose uptake (33), suggesting a similarity in the activity of the arabinose and galactose transporter.

Finally, the 7th suppressor gene we identified, *vc2689*, codes for a homologue of the *E. coli* 6-phosphofructokinase PfkA, a key enzyme in the glycolysis pathway (34) (Figure 5).

Taken together, these results suggest that L-Ara arrests the metabolism of *V. cholerae* because it is mistakenly recognized as a substrate of the Leloir metabolic pathway and that through a series of enzymatic reactions it is converted into a phosphorylated sugar by-product that cannot be further metabolized (Figure 5). Likewise, several studies previously suggested that accumulation of a phosphate ester metabolite could perturb growth: L-Ara inhibits the growth of *E. coli araD* mutants because of the accumulation of L-ribulose 5-phosphate (35); Galactose inhibits the growth of *E. coli galT* mutants because of the accumulation of galactose 1-phosphate (36, 37); Rhamnose stops the growth of *Salmonella* Typhi strains defective in the rhamnose degradation pathway because of the accumulation of L-rhamnulose 1-phosphate (35, 38).

L-Ara mediated metabolic perturbation does not prevent the use of P_{BAD}

Importantly, the realization that L-Ara can perturb the metabolism of *V. cholerae* does not jeopardize previous results obtained with the *E. coli* P_{BAD} expression system in this bacterium since L-Ara concentrations lower than those that promote growth arrest and spheroplasts formation are almost always used (Figure 1). However, our study indicates that special care should be taken in future works when using the *E. coli* P_{BAD} expression system in mutants of *V. cholerae* (Figure 1). It also shows how metabolic artefacts linked to L-Ara can be avoided by performing experiments in cells that can import L-Ara but are insensitive to it by mutation of *vc1595*, which codes for the first enzyme probably processing L-Ara in the cytoplasm (Figure 4 and 5).

Spheroplasts formation results from an imbalance in cell wall degradation and synthesis

The analysis of the muropeptide composition of L-Ara treated *V. cholerae* cells showed that they still maintained a residual amount of PG whose structure was remarkably similar to that described for *E. coli* cefsulodin-induced L-forms (39). The dramatic decrease in the average chain-length and corresponding increase in anhydro-muropeptides hint to a higher activity of

346 lytic transglycosylases in cleaving the PG and producing shorter chains. The increase in DAP-
347 DAP cross-linkage, an unusual kind of cross-linkage specifically generated by L,D-
348 transpeptidases (40), further suggests that the metabolic arrest induced by L-Ara affects PBPs
349 activity and stimulates transpeptidation mediated by the L,D-transpeptidase LdtA (41). Taken
350 together, these results suggest that L-Ara promotes the formation of spheroplasts because it
351 induces a metabolic arrest that leads to an imbalance between PG synthesis and degradation.
352 Interestingly, one of the suppressors we identified in the Tn screenings (*vc2689*) codes for a
353 homologue of the glycolytic enzyme PfkA, whose normal metabolic substrate, phosphor-
354 sugar fructose 6-phosphate, is an essential precursor for UDP-GlcNAc and subsequently
355 Lipid II and PG synthesis through the GlmS pathway (42) (Figure 5). It suggests that the
356 imbalance between PG synthesis and degradation might result from the depletion or
357 replacement of phosphor-sugar fructose 6-phosphate by a by-product of L-Ara and/or by the
358 poisoning of GlmS.

359 **WigKR dependent up-regulation of cell wall synthesis genes is essential for recovery**

360 Like L-Ara, antibiotics inhibiting cell wall synthesis promote the formation of viable
361 spheroplasts that can revert to the original cell shape after a few divisions when the antibiotics
362 are removed (5). However, in contrast to L-Ara induced spheroplasts, *V. cholerae* cells
363 exposed to antibiotics inhibiting cell wall synthesis grow in volume over time, suggesting that
364 they are not dormant (Figure 3, (43, 44)). In this regard, antibiotic treated cells are more
365 similar to bacterial L-forms, which can be obtained in osmotic stabilizing media in several
366 microorganisms, including *E. coli*, by treating cells with lysozyme (45), by adding the β-
367 lactam cefsulodin (a specific inhibitor of the penicillin binding proteins PBP1A and PBP1B)
368 (39, 46), or by inhibiting synthesis of the Lipid II cell wall precursor with fosfomycin (47).
369 The spheroplasts induced by the treatment of Δ*wigKR* cells by L-Ara increased in volume
370 when L-Ara was removed from the growth media, demonstrating that cell metabolism was

very rapidly restored (Figure 3D). However, the expansion in volume of the cells led to lysis (Figure 3D). These results indicate that the recovery of a constitutive level of PG synthesis was not sufficient to expand the residual amount of cell wall left in the spheroplasts to accommodate the increase in cellular material, as observed for the spheroplasts induced by cell wall targeting antibiotics. These results fit with the idea that the histidine kinase/response regulator pair WigKR dependent up-regulation of the full set of cell wall synthetic genes is necessary for cell shape recovery of *V. cholerae* spheroplasts (25).

L-Ara sensitivity is a common feature of *Vibrios*

L-Ara induced spheroplasts formation and inhibition of cell growth is observed in clinically relevant O1 and O139 strains as well as in environmental non-O1 non-O139 strains (Supplementary Figure 3 and (15)).

Interestingly, it was shown that L-Ara induced biofilm formation and had an inhibitory effect on cell growth in *Vibrio fischeri* (48). No remarks were made about cell morphology. However, mutations in GalK or the galactose transporter were found to suppress the phenomenon, as observed for the action of L-Ara in *V. cholerae* (48). Thus, L-Ara sensitivity could be a phenotype shared by different species of *Vibrios*.

Methods

Plasmids and strains

Bacterial strains and plasmids used in this study are listed in Table 4. Strains were rendered competent by the insertion of *hapR* by specific transposition and constructed by natural transformation. Engineered strains were confirmed by PCR. Primers are listed in Supplementary Table 1.

Growth curves

If not otherwise indicated, cells were grown at 30°C in M9 minimal medium supplemented with 0.2% (w/v) fructose and 1 µg/ml thiamine (M9-MM), M9-MM + 0.1% casamino acids

(M9-MM + CAA) and Luria-Bertani broth (LB) in a 96-well microtiter plate and the optical density at 600 nm followed over time in a Tecan plate reader. The growth curves plotted are the average of three replicates; the standard deviation is represented for each time point. For CFU and rod to sphere kinetics, cells were grown in flasks in M9-MM at 30°C and 37°C, 0.2% (w/v) L-Ara was added when indicated. Samples were taken every hour for plating and/or microscopic inspection. Three replicates were performed for each experiment. L-Ara was added to cell cultures with an OD_{600} comprised between 0.02 and 0.05.

L-Ara survival assay

Over-night wild-type (EPV50) and Δ*wigKR* (EGV515) cultures were diluted 200 times in M9-MM, followed by 2 hours of growth at 30°C before 0.2% (w/v) L-Ara was added. Cells were checked for transition to spherical morphology at the microscope. Serial dilutions of T_0 (before L-Ara addition) and T_{10} (after L-Ara treatment) samples were plated on LB plates and the number of colonies used to calculate the CFU at T_0 and T_{10}. The ratio CFU T_{10} / CFU T_0 is used to calculate the percentage of cells able to survive L-Ara treatment and revert to proliferation.

Microscopy

Cells were spread on a 1% (w/v) agar pad (ultrapure agarose, Invitrogen) for analysis. For snapshots, images were acquired using a DM6000-B (Leica) microscope. For time-lapse analyses the agarose pad was made using M9-MM with 0.2% (w/v) L-Ara if needed and images were acquired using an Evolve 512 EMCCD camera (Roper Scientific) attached to an Axio Observe spinning disk (Zeiss). To observe rod to sphere transition on agarose pads, 0.2% (w/v) L-Ara was added in liquid M9-MM cultures 2 hours before transferring cells on agarose pads containing L-Ara and starting microscopic imaging.

Transposon insertion deep sequencing-based screen

The Tn library was constructed in an EPV50 background and libraries for Illumina sequencing were prepared as described in Espinosa *et al*. (49). Aliquots of the transposon library were thawed on ice and ~10^9 cells were diluted into 100 ml of M9-MM and grown for 1 hour at 30°C before adding 0.2% (w/v) L-Ara. The culture was incubated at 30°C in a shacking incubator for additional 18 hours. Samples for library construction and deep sequencing were collected before L-Ara addition and after 9 and 18 hours of incubation with L-Ara.

Tn-seq analysis

Cutadapt was used to remove adapters and transposon sequences. Genome sequences were mapped using bwa as described in (50, 51). Transposon insertions were visualized using the Artemis browser (52).

Transposon mutagenesis screen on plate

The transposon mutagenesis was performed conjugating the *E. coli* strain SM10 λ *pir*/pSC189, which carries a mini-Himar transposon associated to a kanamycin resistance, with the *V. cholerae* strain EGV299. In detail, 1 ml of culture of EGV299 grown to OD_{600} 0.3 was mixed with 100 µl of donor strain SM10 λ *pir* carrying the transposon donor plasmid pSC189 grown to OD_{600} 0.5. Each mixture was pelleted, resuspended and deposited onto a 0.45 µm filter (Millipore) on a LB agar plate supplemented with DAP. Conjugation was carried out for 6 hours at 37°C and then cells were pooled together and plated directly on M9-MM plates containing kanamycin and 0.1% (w/v) L-Ara and incubated over night at 30°C. Eight conjugations were performed per each library. We constructed two Tn libraries of approximately 300,000 clones each. Mutants able to grow on plate were isolated and inspected at the microscope for growth and morphology in presence of L-Ara. An arbitrary PCR followed by DNA sequencing was performed to determine the Tn insertion site.

Peptidoglycan analysis

EGV217 over-night cultures were diluted 200 times in M9-MM and grown at 30°C. 100 ml were centrifuged after 7 hours of growth and 1 L of culture, to which 0.2% (w/v) L-Ara was added after 2 hours, was harvested after further 7 hours of incubation. Cells were checked for complete transition to spherical morphology at the microscope before harvesting. Previously described methods were followed for muropeptide isolation and ultra-performance liquid chromatography (UPLC) analysis (53, 54). After boiling for 2 hours cell pellets with SDS (sodium dodecyl sulfate), the lysates were left stirring over night at room temperature. Cell wall material was pelleted, washed with MQ water to remove the SDS, and digested with pronase E to remove Braun's lipoprotein. Purified peptidoglycan was re-suspended in MQ water and treated over night with muramidase at 37°C. Soluble muropeptides were reduced with sodium borohydride and the pH then adjusted to 3.5 with phosphoric acid. Samples were injected in an UPLC system to obtain the muropeptide profiles. UPLC separation was performed on a Waters UPLC system equipped with an ACQUITY UPLC BEH C18 Column, 130 Å, 1.7 µm, 2.1 mm × 150 mm (Waters) and a dual wavelength absorbance detector using a linear gradient from buffer A (phosphate buffer 50 mM, pH 4.35) to buffer B (phosphate buffer 50 mM, pH 4.95, methanol 15% (v/v)) in a 28-min run with a 0.25 ml/min flow. Elution of muropeptides was detected at 204 nm. Identity of the peaks was assigned by comparison of the retention times and profiles to other chromatograms in which mass spectrometry data have been collected. The relative amounts of the muropeptides and the percentage of cross-linkage were calculated as described by Glauner *et al*. (22). To estimate the amount of peptidoglycan per cell, the total area of the chromatogram was normalized to the OD of the culture. All values are the means of three independent experiments.

Figures and Tables Legends

Figure 1. L-Ara induces loss of rod shape. A. Phase contrast images of *V. cholerae* N16961 cells (strain EPV50) grown at 30°C in the indicated media with increasing concentrations of L-Ara. **B.** Phase contrast images of *V. cholerae* N16961 cells (strain EPV50) incubated in M9-MM at 4°C for 6 weeks (left panel) and grown in LB with 100 µM Ampicillin (Amp) at 30°C (right panel). **C.** Phase contrast images of *V. cholerae* strain EGV299 (MCH1 P_{BAD}*::YGFP-slmA*) and EGV300 (N16961 P_{BAD}*::ssb-YGFP*) cells grown in M9-MM at 30°C in presence of 0.01% (w/v) L-Ara. Scale bars = 2 µm.

Figure 2. Transition dynamics to spherical cells. Cells of *V. cholerae* strain EPV50 were grown in M9-MM at 30°C. L-Ara was added at a concentration of 0.2% (w/v) when indicated. **A.** Kinetics of *V. cholerae* morphological change from rods to spherical cells. Cell shape was inspected at the microscope every hour after L-Ara addition. A representative image for each cell category (rod, transitioning, spherical) is represented. Mean of three independent replicates and the standard deviation are represented. **B.** Diameter distribution of *V. cholerae* spherical cells treated with L-Ara for 10 hours. **C.** Average diameter of *V. cholerae* spherical cells over time. Mean of three independent replicates and the standard deviation are represented. **D.** Transition from rods to spherical forms. EPV50 cells were mounted on a M9-MM agarose pad containing 0.2% (w/v) L-Ara. Bright-field still images from time-lapse microscopy experiments. Images were taken every 5 minutes for 12.5 hours. Scale bars = 2 µm.

Figure 3. Recovery of growth and rod shape. Cells were grown in M9-MM at 30°C. L-Ara was added at a concentration of 0.2% (w/v) when indicated. Viable colony count (CFU) of *V. cholerae* cells (strain EPV50) grown with and without L-Ara over time (**A**) and after 10 hours (**B**). Mean of three independent replicates and the standard deviation are represented. In the time-lapse experiments, cells were grown in M9-MM + 0.2% (w/v) L-Ara until they became

492 spherical and then mounted on a M9-MM agarose pad in the absence of L-Ara. Bright-field
493 still images were taken every 5 minutes for 14 hours. **C**. N16961 cells (strain EPV50) rod
494 shape recovery. **D.** Spherical Δ*wigKR* cells (strain EGV515) are not able to recover rod shape.
495 Scale bars = 2 µm.

496 **Figure 4. Transposon insertion mutants insensitive to L-Ara-induced cell growth arrest.**
497 Tn-seq profile of a transposon insertion library in an EPV50 background before (top panel)
498 and after incubation with 0.2% (w/v) L-Ara (middle panel for 9 hours and bottom panel for 18
499 hours). Transposon insertion profile of chromosome 1 is shown in (**A**). Chromosomal
500 positions are indicated below. Regions with overrepresented transposon insertions in the
501 presence of L-Ara are shown at the bottom and zoomed in (**B**). Transposon insertion in
502 forward and reverse orientation are indicated by orange and blue vertical lines, respectively.

503 **Figure 5. L-Ara insensitive mutants.** Schematic representation of the galactose and
504 glycolytic metabolic pathways. In red are the genes identified in the Tn screens. The number
505 of Tn insertion (hits) obtained in the screen on plate are specified in between parentheses.
506 Depletion or replacement of D-fructose 6-phosphate by a by-product of L-Ara and/or by the
507 poisoning of GlmS could affect Lipid II synthesis (in blue) and originate cell wall deficient
508 cells.

509 **Table 1.** Carbon sources tested for N16961 (strain EPV50) rod shape loss. They were added
510 to M9-MM at a concentration of 0.2% (w/v), with the exception of glycerol at 10 % (v/v).

511 **Table 2.** Quantification of muropeptides, peptidoglycan cross-linking levels and average
512 chain length of L-Ara treated and non-treated *V. cholerae* cells (strain EGV217). Values are
513 the means of three independent experiments and the standard deviation is represented. *:
514 $p<0.05$ (t-test with a Two-tailed distribution).

515 **Table 3.** Suppressor mutants of L-Ara induced growth arrest identified in a Tn-based screen
516 on plate. The screening was performed in *V. cholerae* strain EGV299.

Table 4. List of bacterial strains and plasmids used in this study.

Data Availability

Tn-seq data are available in the ArrayExpress database (https://www.ebi.ac.uk/arrayexpress) under accession number E-MTAB-9747.

Acknowledgements

We would like to acknowledge financial support from the Agence Nationale pour la Recherche [ANR19-CE35-0013-01 SurVi]. We thank C. Possoz for helpful discussions and Y. Yamaichi for providing the ordered *V. cholerae* mapped Tn library. Research in the Cava laboratory is supported by the Laboratory of Molecular Infection Medicine Sweden (MIMS), the Swedish Research Council (VR), the Knut and Alice Wallenberg Foundation (KAW) and the Kempe Foundation. S.B.H. was supported by a Martin Escudero Postdoctoral fellowship.

References

1. 2006. The Biology of *Vibrios*. American Society of Microbiology.

2. Chaiyanan S, Chaiyanan S, Grim C, Maugel T, Huq A, Colwell RR. 2007. Ultrastructure of coccoid viable but non-culturable *Vibrio cholerae*. Environmental Microbiology 9:393–402.

3. Huq A, Colwell RR, Rahman R, Ali A, Chowdhury MA, Parveen S, Sack DA, Russek-Cohen E. 1990. Detection of *Vibrio cholerae* O1 in the aquatic environment by fluorescent-monoclonal antibody and culture methods. 8. Appl Environ Microbiol 56:2370–2373.

4. Alam M, Sultana M, Nair GB, Siddique AK, Hasan NA, Sack RB, Sack DA, Ahmed KU, Sadique A, Watanabe H, Grim CJ, Huq A, Colwell RR. 2007. Viable but

nonculturable *Vibrio cholerae* O1 in biofilms in the aquatic environment and their role in cholera transmission. Proc Natl Acad Sci USA 104:17801–17806.

5. Dörr T, Davis BM, Waldor MK. 2015. Endopeptidase-mediated beta lactam tolerance. PLoS Pathog 11:e1004850.

6. Clemens JD, Nair GB, Ahmed T, Qadri F, Holmgren J. 2017. Cholera. Lancet 390:1539–1549.

7. Chun J, Grim CJ, Hasan NA, Lee JH, Choi SY, Haley BJ, Taviani E, Jeon YS, Kim DW, Brettin TS, Bruce DC, Challacombe JF, Detter JC, Han CS, Munk AC, Chertkov O, Meincke L, Saunders E, Walters RA, Huq A, Nair GB, Colwell RR. 2009. Comparative genomics reveals mechanism for short-term and long-term clonal transitions in pandemic *Vibrio cholerae*. Proc Natl Acad Sci U S A 106:15442–7.

8. Weill F-X, Domman D, Njamkepo E, Tarr C, Rauzier J, Fawal N, Keddy KH, Salje H, Moore S, Mukhopadhyay AK, Bercion R, Luquero FJ, Ngandjio A, Dosso M, Monakhova E, Garin B, Bouchier C, Pazzani C, Mutreja A, Grunow R, Sidikou F, Bonte L, Breurec S, Damian M, Njanpop-Lafourcade B-M, Sapriel G, Page A-L, Hamze M, Henkens M, Chowdhury G, Mengel M, Koeck J-L, Fournier J-M, Dougan G, Grimont PAD, Parkhill J, Holt KE, Piarroux R, Ramamurthy T, Quilici M-L, Thomson NR. 2017. Genomic history of the seventh pandemic of cholera in Africa. Science 358:785–789.

9. Domman D, Quilici M-L, Dorman MJ, Njamkepo E, Mutreja A, Mather AE, Delgado G, Morales-Espinosa R, Grimont PAD, Lizárraga-Partida ML, Bouchier C, Aanensen DM, Kuri-Morales P, Tarr CL, Dougan G, Parkhill J, Campos J, Cravioto A, Weill F-X, Thomson NR. 2017. Integrated view of *Vibrio cholerae* in the Americas. Science 358:789–793.

562 10. Mutreja A, Kim DW, Thomson NR, Connor TR, Lee JH, Kariuki S, Croucher NJ, Choi
563 SY, Harris SR, Lebens M, Niyogi SK, Kim EJ, Ramamurthy T, Chun J, Wood JLN,
564 Clemens JD, Czerkinsky C, Nair GB, Holmgren J, Parkhill J, Dougan G. 2011. Evidence
565 for several waves of global transmission in the seventh cholera pandemic. Nature
566 477:462–465.

567 11. Kim EJ, Lee D, Moon SH, Lee CH, Kim SJ, Lee JH, Kim JO, Song M, Das B, Clemens
568 JD, Pape JW, Nair GB, Kim DW. 2014. Molecular Insights Into the Evolutionary
569 Pathway of *Vibrio cholerae* O1 Atypical El Tor Variants. PLoS Pathog 10:e1004384.

570 12. Guzman LM, Belin D, Carson MJ, Beckwith J. 1995. Tight regulation, modulation, and
571 high-level expression by vectors containing the arabinose PBAD promoter. 14. J Bacteriol
572 177:4121–30.

573 13. Dalia TN, Chlebek JL, Dalia AB. 2020. A modular chromosomally integrated toolkit for
574 ectopic gene expression in *Vibrio cholerae*. Sci Rep 10:15398.

575 14. Lee N, Francklyn C, Hamilton EP. 1987. Arabinose-induced binding of AraC protein to
576 *araI2* activates the *araBAD* operon promoter. Proc Natl Acad Sci USA 84:8814–8818.

577 15. Golder T, Mukhopadhyay AK, Koley H, Nandy RK. 2020. Nonmetabolizable arabinose
578 inhibits *Vibrio cholerae* growth in M9 medium with gluconate as sole carbon source. Jpn
579 J Infect Dis https://doi.org/10.7883/yoken.JJID.2019.304.

580 16. E. Galli, E. Espinosa, F.X. Barre. L-Arabinose and uses thereof against *Vibrio* genus
581 bacteria. EP17305197.0.

582 17. Oliver JD. 2010. Recent findings on the viable but nonculturable state in pathogenic
583 bacteria. FEMS Microbiol Rev 34:415–425.

584 18. Shiba T, Hill RT, Straube WL, Colwell RR. 1995. Decrease in culturability of *Vibrio*
585 *cholerae* caused by glucose. Appl Environ Microbiol 61:2583–2588.

586 19. Bianco PR, Lyubchenko YL. 2017. SSB and the RecG DNA helicase: an intimate
587 association to rescue a stalled replication fork. Protein Sci 26:638–649.

588 20. Galli E, Poidevin M, Le Bars R, Desfontaines J-M, Muresan L, Paly E, Yamaichi Y,
589 Barre F-X. 2016. Cell division licensing in the multi-chromosomal *Vibrio cholerae*
590 bacterium. Nature Microbiology 1:16094.

591 21. Allan EJ, Hoischen C, Gumpert J. 2009. Bacterial L-forms. Adv Appl Microbiol 68:1–
592 39.

593 22. Glauner B, Höltje JV, Schwarz U. 1988. The composition of the murein of *Escherichia*
594 *coli*. J Biol Chem 263:10088–10095.

595 23. van Heijenoort J. 2011. Peptidoglycan hydrolases of *Escherichia coli*. Microbiol Mol
596 Biol Rev 75:636–663.

597 24. Vollmer W, Joris B, Charlier P, Foster S. 2008. Bacterial peptidoglycan (murein)
598 hydrolases. FEMS Microbiol Rev 32:259–286.

599 25. Dörr T, Alvarez L, Delgado F, Davis BM, Cava F, Waldor MK. 2016. A cell wall
600 damage response mediated by a sensor kinase/response regulator pair enables beta-
601 lactam tolerance. Proc Natl Acad Sci USA 113:404–409.

602 26. van Opijnen T, Bodi KL, Camilli A. 2009. Tn-seq: high-throughput parallel sequencing
603 for fitness and genetic interaction studies in microorganisms. Nat Methods 6:767–772.

604 27. Cameron DE, Urbach JM, Mekalanos JJ. 2008. A defined transposon mutant library and
605 its use in identifying motility genes in *Vibrio cholerae*. Proc Natl Acad Sci USA
606 105:8736–8741.

607 28. Harayama S, Bollinger J, Iino T, Hazelbauer GL. 1983. Characterization of the *mgl*
608 operon of *Escherichia coli* by transposon mutagenesis and molecular cloning. J Bacteriol
609 153:408–415.

610 29. Hogg RW, Voelker C, Von Carlowitz I. 1991. Nucleotide sequence and analysis of the
611 *mgl* operon of *Escherichia coli* K12. Mol Gen Genet 229:453–459.

612 30. Kalckar HM, Kurahashi K, Jordan E. 1959. Hereditary defects in galactose metabolism
613 in *Escherichia coli* mutants, I. Determination of enzyme activities. Proc Natl Acad Sci
614 USA 45:1776–1786.

615 31. Stevenson G, Andrianopoulos K, Hobbs M, Reeves PR. 1996. Organization of the
616 *Escherichia coli* K-12 gene cluster responsible for production of the extracellular
617 polysaccharide colanic acid. J Bacteriol 178:4885–4893.

618 32. Patel KB, Toh E, Fernandez XB, Hanuszkiewicz A, Hardy GG, Brun YV, Bernards MA,
619 Valvano MA. 2012. Functional characterization of UDP-glucose:undecaprenyl-
620 phosphate glucose-1-phosphate transferases of *Escherichia coli* and *Caulobacter*
621 *crescentus*. J Bacteriol 194:2646–2657.

622 33. Geddes BA, Oresnik IJ. 2012. Inability to catabolize galactose leads to increased ability
623 to compete for nodule occupancy in *Sinorhizobium meliloti*. J Bacteriol 194:5044–5053.

624 34. Babul J. 1978. Phosphofructokinases from *Escherichia coli*. Purification and
625 characterization of the nonallosteric isozyme. J Biol Chem 253:4350–4355.

626 35. Englesberg E, Anderson RL, Weinberg R, Lee N, Hoffee P, Huttenhauer G, Boyer H.
627 1962. L-Arabinose-sensitive, L-ribulose 5-phosphate 4-epimerase-deficient mutants of
628 *Escherichia coli*. J Bacteriol 84:137–146.

629 36. Kurahashi K, Wahba AJ. 1958. Interference with growth of certain *Escherichia coli*
630 mutants by galactose. Biochim Biophys Acta 30:298–302.

631 37. Yarmolinsky MB, Wiesmeyer H, Kalckar HM, Jordan E. 1959. Hereditary defects in
632 galactose metabolism in *Escherichia coli* mutants, II. Galactose-induced sensitivity. Proc
633 Natl Acad Sci USA 45:1786–1791.

634 38. Englesberg E, Baron LS. 1959. Mutation to L-rhamnose resistance and transduction to
635 L-rhamnose utilization in *Salmonella typhosa*. J Bacteriol 78:675–686.

636 39. Joseleau-Petit D, Liébart J-C, Ayala JA, D'Ari R. 2007. Unstable *Escherichia coli* L
637 forms revisited: growth requires peptidoglycan synthesis. J Bacteriol 189:6512–6520.

638 40. Magnet S, Dubost L, Marie A, Arthur M, Gutmann L. 2008. Identification of the L,D-
639 transpeptidases for peptidoglycan cross-linking in *Escherichia coli*. J Bacteriol
640 190:4782–4785.

641 41. Cava F, de Pedro MA, Lam H, Davis BM, Waldor MK. 2011. Distinct pathways for
642 modification of the bacterial cell wall by non-canonical D-amino acids. EMBO J
643 30:3442–3453.

644 42. Milewski S. 2002. Glucosamine-6-phosphate synthase--the multi-facets enzyme.
645 Biochim Biophys Acta 1597:173–192.

646 43. Weaver AI, Murphy SG, Umans BD, Tallavajhala S, Onyekwere I, Wittels S, Shin J-H,
647 VanNieuwenhze M, Waldor MK, Dörr T. 2018. Genetic Determinants of Penicillin
648 Tolerance in *Vibrio cholerae*. Antimicrob Agents Chemother 62.

649 44. Cross T, Ransegnola B, Shin J-H, Weaver A, Fauntleroy K, VanNieuwenhze MS,
650 Westblade LF, Dörr T. 2019. Spheroplast-Mediated Carbapenem Tolerance in Gram-
651 Negative Pathogens. Antimicrob Agents Chemother 63.

652 45. Ranjit DK, Young KD. 2013. The Rcs stress response and accessory envelope proteins
653 are required for de novo generation of cell shape in *Escherichia coli*. J Bacteriol
654 195:2452–2462.

655 46. Cambré A, Zimmermann M, Sauer U, Vivijs B, Cenens W, Michiels CW, Aertsen A,
656 Loessner MJ, Noben J-P, Ayala JA, Lavigne R, Briers Y. 2015. Metabolite profiling and
657 peptidoglycan analysis of transient cell wall-deficient bacteria in a new *Escherichia coli*
658 model system. Environ Microbiol 17:1586–1599.

659 47. Mercier R, Kawai Y, Errington J. 2014. General principles for the formation and
660 proliferation of a wall-free (L-form) state in bacteria. Elife 3.

661 48. Visick KL, Quirke KP, McEwen SM. 2013. Arabinose induces pellicle formation by
662 *Vibrio fischeri*. Appl Environ Microbiol 79:2069–2080.

663 49. Espinosa E, Paly E, Barre F-X. 2020. High-Resolution Whole-Genome Analysis of
664 Sister-Chromatid Contacts. Mol Cell 79:857-869.e3.

665 50. Li H, Durbin R. 2010. Fast and accurate long-read alignment with Burrows-Wheeler
666 transform. Bioinformatics 26:589–595.

667 51. Martin M. 2011. Cutadapt removes adapter sequences from high-throughput sequencing
668 reads. 1. EMBnet.journal 17:10–12.

669 52. Carver T, Harris SR, Berriman M, Parkhill J, McQuillan JA. 2012. Artemis: an
670 integrated platform for visualization and analysis of high-throughput sequence-based
671 experimental data. Bioinformatics 28:464–469.

672 53. Desmarais SM, De Pedro MA, Cava F, Huang KC. 2013. Peptidoglycan at its peaks:
673 how chromatographic analyses can reveal bacterial cell wall structure and assembly. Mol
674 Microbiol 89:1–13.

675 54. Möll A, Dörr T, Alvarez L, Davis BM, Cava F, Waldor MK. 2015. A D, D-
676 carboxypeptidase is required for *Vibrio cholerae* halotolerance. Environ Microbiol
677 17:527–540.

678 55. David A, Demarre G, Muresan L, Paly E, Barre F-X, Possoz C. 2014. The two *Cis*-
679 acting sites, *parS1* and *oriC1*, contribute to the longitudinal organisation of *Vibrio*
680 *cholerae* chromosome I. PLoS Genet 10:e1004448.

681 56. Simon R, Priefer U, Puhler A. 1983. A Broad Host Range Mobilization System for *In*
682 *Vivo* Genetic Engineering: Transposon Mutagenesis in Gram Negative Bacteria. Nat
683 Biotech 1:784–791.

684 57. Chiang SL, Rubin EJ. 2002. Construction of a mariner-based transposon for epitope-
685 tagging and genomic targeting. Gene 296:179–85.

686

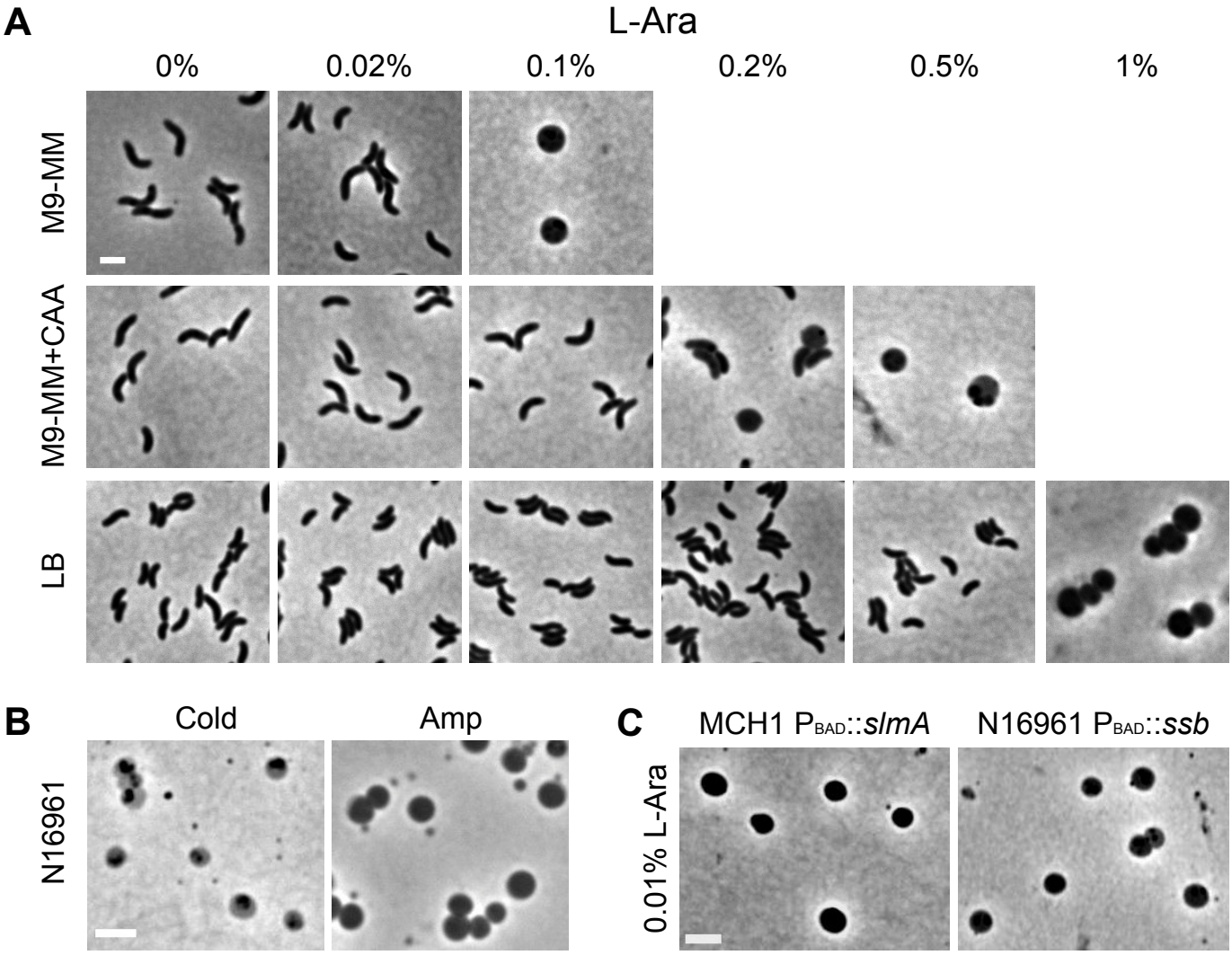

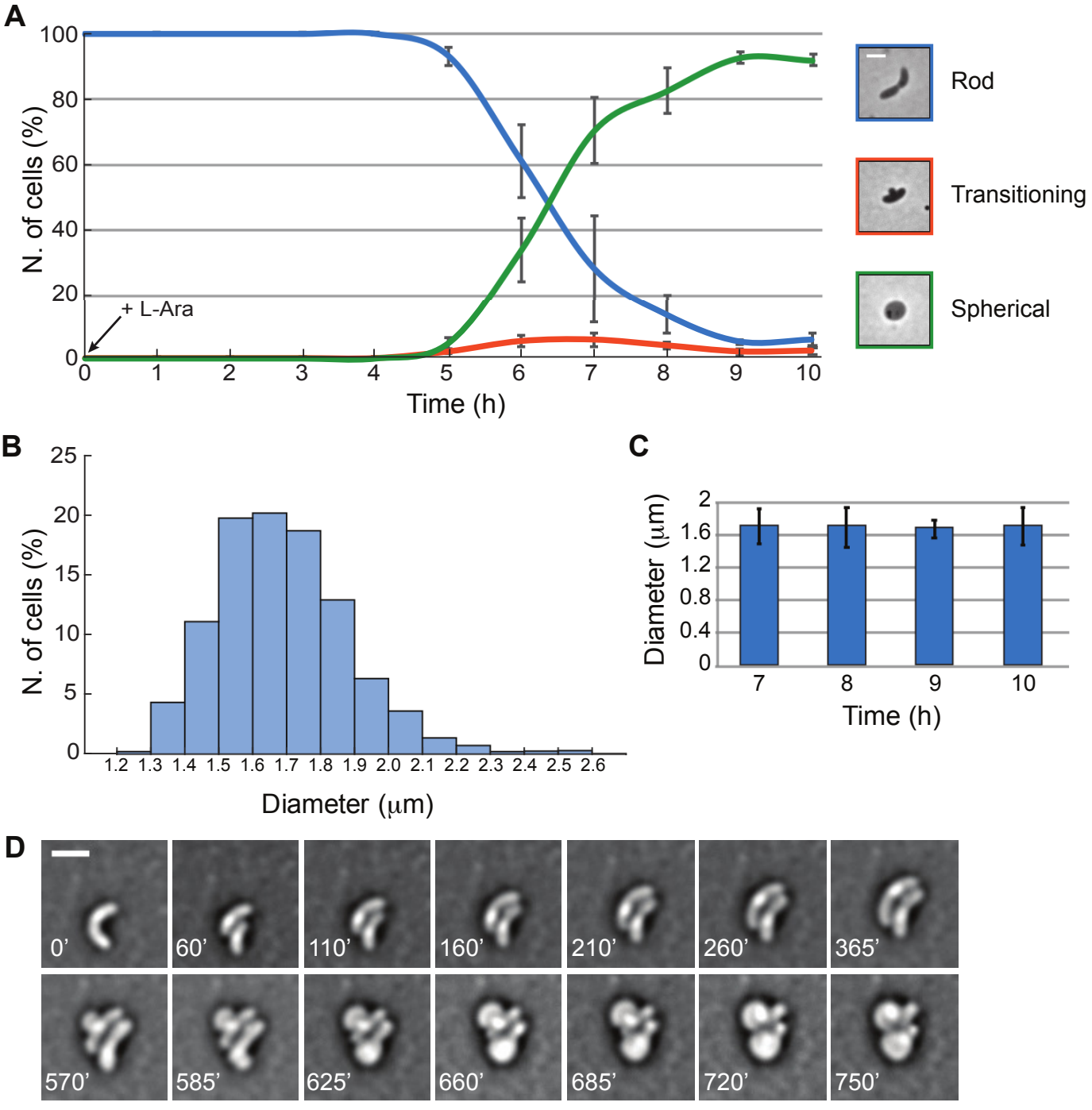

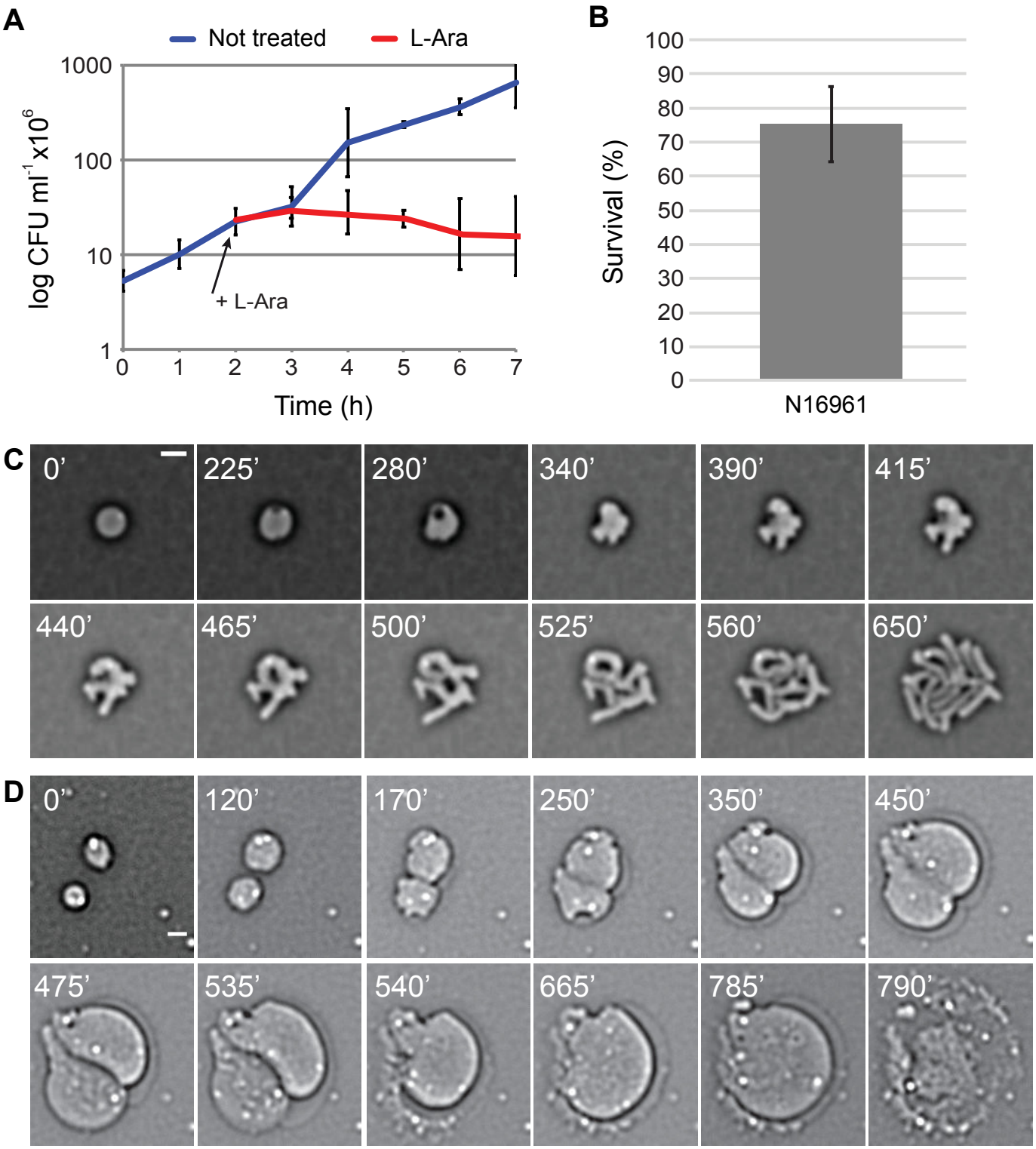

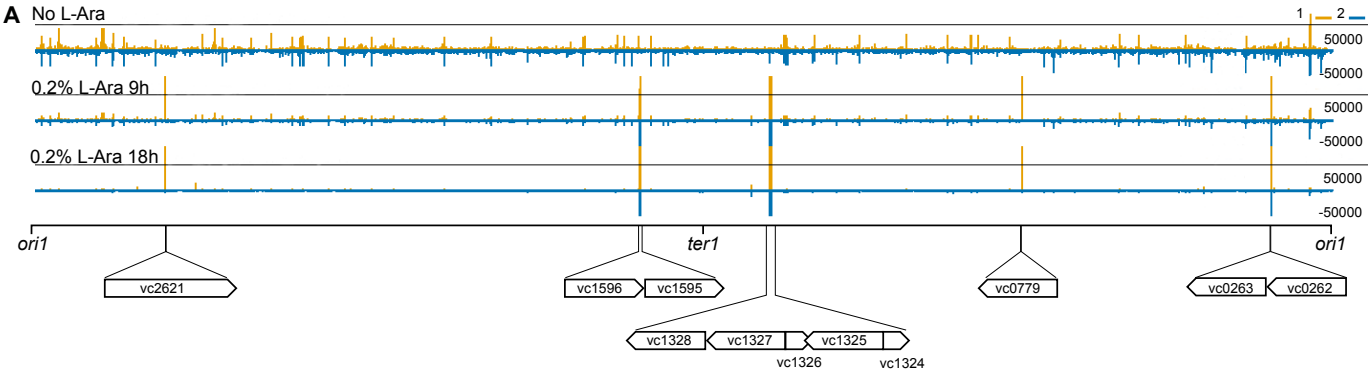

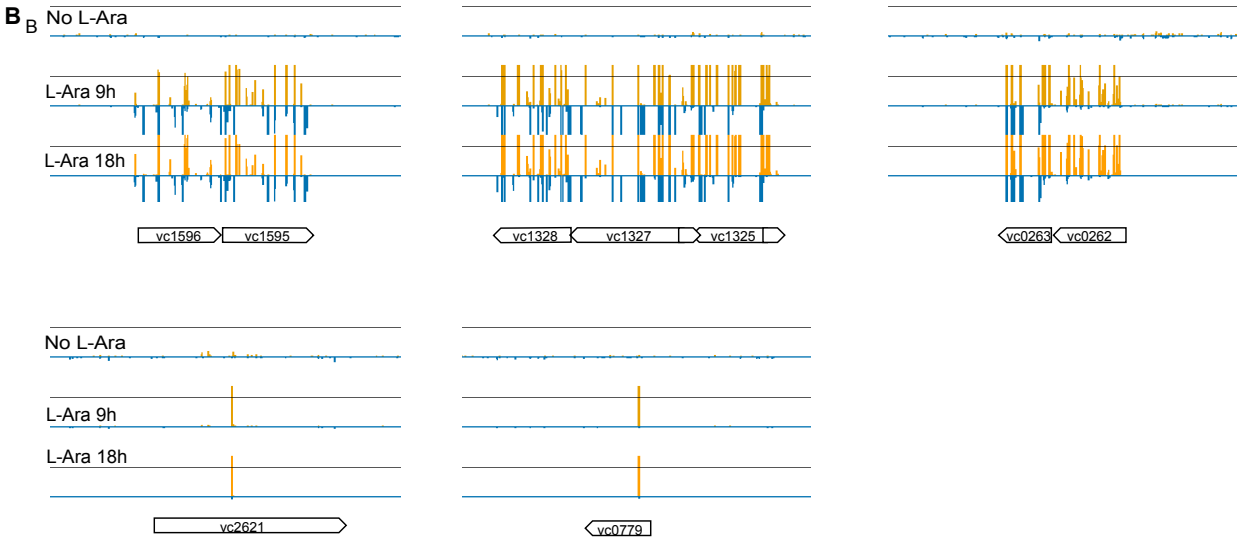

D-galactose ABC transporter: VC1325 (1 hit), VC1327 (1 hit), VC1328 (1 hit)

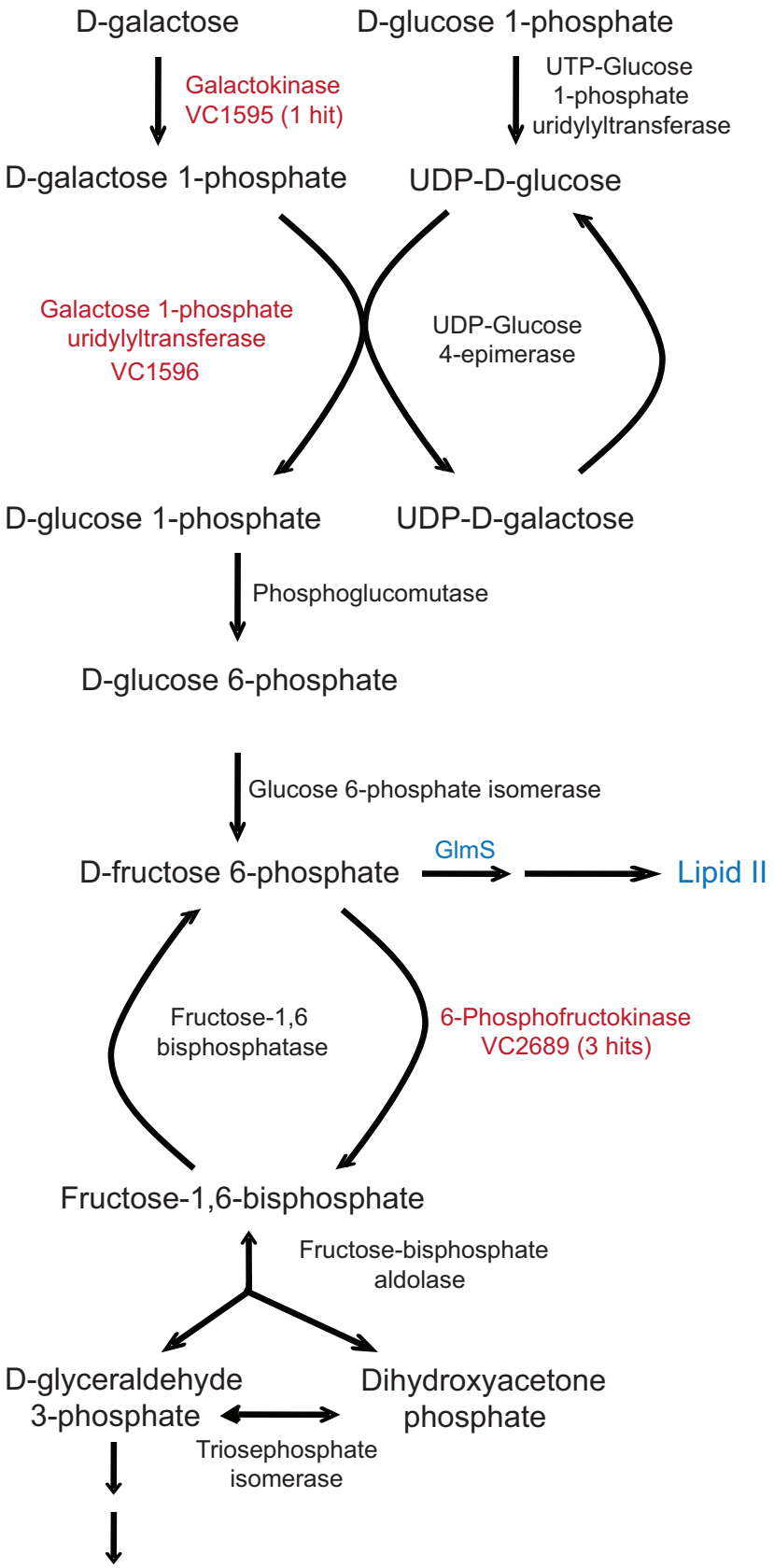

Applied and Environmental Microbiology

Tables

Table 1.

Carbon source	Growth	Spherical cells
D-Arabinose	+	−
L-Arabinose	−	+
L-Rhamnose	+	−
D-Glucose	+	−
D-Galactose	+	−
Glycerol	+	−
D-Sucrose	+	−
D-Xylose	+	−
Succinate	+	−

Table 2.

Muropeptide group	**Non-treated**	**L-Ara-treated**
*Monomers (%)	48.1 (±0.6)	40.2 (±3.2)
Dimers (%)	43.1 (±1.9)	47.2 (±3.1)
Trimers (%)	8.8 (±2.5)	12.6 (±4.8)
*Anhydro-muropeptides (%)	14.8 (±2.3)	21.9 (±3.7)
*DAP-DAP cross-linked muropeptides (%)	4.9 (±0.7)	7.5 (±0.9)
Peptidoglycan feature	**Non-treated**	**L-Ara-treated**
*Total cross-linkage (%)	37.7 (±1.4)	47.2 (±5.0)
*Average glycan chain length	11.7 (±1.4)	7.5 (±1.1)

Table 3.

Gene	Putative function	N. hits
vc0263	Galactosyl-transferase	2
vc1325	Galactoside ABC transporter, periplasmic D-galactose/D-glucose binding protein	1
vc1327	Galactoside ABC transporter, ATP-binding protein	1
vc1328	Galactoside ABC transporter, permease protein	1
vc1595	Galactokinase	1
vc2689	6-Phosphofructokinase, isozyme I	3

Table 4.

Name	Relevant genotype or features	Reference
V. cholerae 104154	wild-type strain, non-O1 non-O139 serogroup	Lab. collection
V. cholerae C6706	wild-type strain, O1 serogroup	Lab. collection
V. cholerae E7946	wild-type strain, O1 serogroup	Lab. collection
V. cholerae EGV217	MCH1 *ChapR ΔlacZ::*(P_{BAD}*::YGFP-slmA-Sh ble*) zeo^R, gm^R	This study
V. cholerae EGV299	MCH1 *ChapR ΔlacZ::*(P_{BAD}*::YGFP-slmA-lacZ-Sh ble*) zeo^R, gm^R	This study
V. cholerae EGV300	N16961 ChapR Δ*lacZ::*(P_{BAD}*::ssb-YGFP-lacZ-Sh ble*) zeo^R, gm^R	This study
V. cholerae EGV515	N16961 *ChapR ΔlacZ wigKR::aadA* $spec^R$, gm^R	This study
V. cholerae EPV50	N16961 *ChapR ΔlacZ* gm^R	(55)
V. cholerae VC0263	C6706 Tn inactivated *vc0263* kan^R	(27)
V. cholerae VC1325	C6706 Tn inactivated *vc1325* kan^R	(27)
V. cholerae VC1327	C6706 Tn inactivated *vc1327* kan^R	(27)
V. cholerae VC1328	C6706 Tn inactivated *vc1328* kan^R	(27)
V. cholerae VC1595	C6706 Tn inactivated *vc1595* kan^R	(27)
V. cholerae VC1596	C6706 Tn inactivated *vc1596* kan^R	(27)
V. cholerae VC2689	N16961 Tn inactivated *vc2689* kan^R	This study
E. coli SM10 λ *pir*	kan^R, *thi-1*, *thr*, *leu*, *tonA*, *lacY*, *supE*, *recA::RP4-2-Tc::Mu*, *pir*	(56)
Plasmid pEG258	P_{BAD}*::YGFP-slmA-Sh ble* flanked by the upstream and downstream regions of *lacZ*; ori pUC; zeo^R amp^R	This study
Plasmid pEG348	P_{BAD}*::YGFP-slmA-lacZ-Sh ble* flanked by the upstream and downstream regions of *lacZ*; ori pUC; zeo^R amp^R	This study
Plasmid pEG352	P_{BAD}*::ssb-YGFP-lacZ-Sh ble* flanked by the upstream and downstream regions of *lacZ*; ori pUC; zeo^R amp^R	This study
Plasmid pEG431	*aadA* flanked by the upstream and downstream regions of	This study

	wigKR; ori p15a; cm^R, $spec^R$	